

Supernovae and Star Formation in M101 and M82

Alice Cheng

June 8, 2023

Abstract

M101 is a spiral galaxy located 21 million light years away. Using the WaSP instrument on the 200-inch Hale Telescope at Palomar Observatory, we imaged M101 under the r', g', i' and h-alpha filters. A recent supernova discovered in the spiral arms of M101 on May 19, 2023 was one of the closest in the past decade. We calculated an upper bound of around 23.77 magnitude under the i' filter for the progenitor of the supernova as the point source itself was not clearly visible due to high levels of noise. We also imaged M82, a starburst galaxy, under the same filters with the same instrument. Using a signal threshold, we estimated the fraction of each galaxy undergoing massive star formation to compare the amount of star formation from M101 with the amount in a starburst galaxy which has an exceptionally high rate of star formation due to gravitational interactions with neighboring galaxies. This allows us to understand some broad differences and similarities between the processes and forces that exist within both galaxies.

1 M101: The Pinwheel Galaxy

1.1 Background

M101 is nearly two times as wide in diameter as our own Milky Way. Because of its proximity, M101 is one of the best known galaxies outside of our own and is believed to contain roughly 100 billion stars similar to our Sun in terms of temperature and lifetime, which could be important in the search for life and understanding the events throughout the lifetime of our own Sun and how it might affect future life on Earth (4). The arms of M101 also contain many active star-forming regions and stellar clusters. Because M101 is close to other galaxies within a galactic group, stars in M101 experience tidal interactions with stars in the other galaxies, so studying the structure and star-formation within M101 can give us insight into the effects of these external forces (5).

1.2 Instruments

To better understand the structure and composition of the stars throughout M101, we used the Wafer-Scale Imager for Prime (WaSP) instrument on the 200-inch Hale Telescope at Palomar Observatory to image M101 under the r', g', i' and h-alpha filters. These filters cover the visible and near-infrared ranges.

1.3 Technical Details

We used the default settings on the WaSP instrument under 4 different filters: g', r', i', and H-alpha. The computed exposure times are shown below.

Since we expect that we will require some overhead time between exposures, we decided to reduce exposure times and trade off with a lower SNR for some of the filters. Our proposed exposure times are:

- g' : 1x120s (SNR=7.03)
- i' : 3x400s (SNR=4.03)
- r' : 1x120s (SNR=3.85)

- H-alpha : 3x360s (SNR=0.504)

To estimate the signal-to-noise ratio achieved for each of these exposure times, we used the following equation:

$$SNR = \frac{R_* \cdot t}{(R_* \cdot t + R_{sky} \cdot t \cdot n_{pix} + RN^2 \cdot n_{pix} + Dark \cdot t \cdot n_{pix})^{\frac{1}{2}}} \quad (1)$$

For the i' and h-alpha images, splitting up images into multiple exposures and then coadding or taking the median rather than taking one extremely long exposure helped reduces the overall amount of noise.

2 Data Reduction

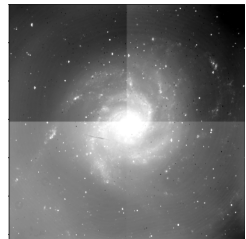
2.1 Calibrations

Our first step in data reduction of images was to take calibration images. Calibration with bias frames is typically used to account for the inherent noise within a telescope and its detector. Flat frames are typically used to quantify the non-uniform sensitivity in the detector. We took 11 bias frames of 0 seconds each and 11 flat frames of the illuminated interior of the dome with an exposure of 10 seconds each. These calibrations were taken in the afternoon, since these calibrations do not require the telescope to be pointed into a dark sky.

The WaSP data was saved into a FITS file. The raw FITS file for one exposure under the i' filter is displayed as an image below, with and without removing the pixels with values in the 1st and 99th percentile (to get rid of noise/hot pixels).



(a) Non-trimmed display



(b) Trimmed display

Figure 1: Raw FITS data of M101 under the i' filter

We then created a master bias and master flat for each filter by taking the median pixel value along the rows (axis 0) across all bias files and flat files, respectively.

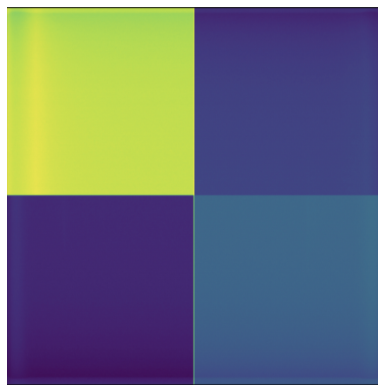


Figure 2: Master Bias



Figure 3: Flat fields under all 4 filters

2.2 Image Reduction

2.2.1 M101

Since we took several exposures under the i' and h-alpha filters, we combined the images. For i' , since the signal in the images was relatively high, we took the median across all exposures. For h-alpha, the signal was a bit lower so we decided to co-add all the images.

We then subtracted the master bias from each of the FITS files for the different filters and divided by the master flat. For creating the images, we also divided each of the images by the exposure time in order to scale the counts in each pixel roughly similar. We then removed outlier pixels by trimming the 1st and 99th percentile from the image. Below are the results of our reduced images under each filter.

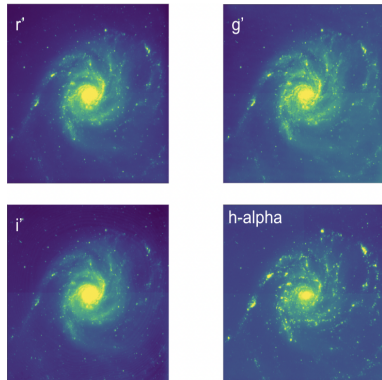


Figure 4: Reduced M101 Images

Finally, we stacked three of the filters on top of each other to generate a false-color image. In the image below, we use the g' , r' , and h-alpha images, with the red indicating the h-alpha portion of the stacked image and therefore highlighting the main star-forming regions of M101 (figure 5).



Figure 5: False-color Image of M101 using g' , r' , h-alpha filters

2.2.2 M82

We reduced images for M82 under i' , r' , g' and h-alpha filters using similar steps as described for M101 image reduction. These can be seen in figures 6 and 7.

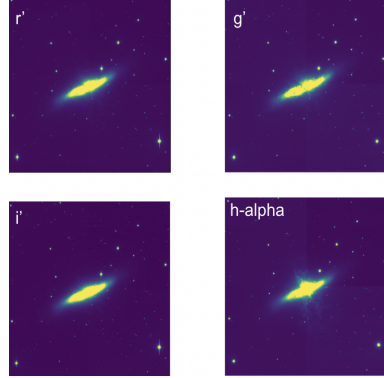


Figure 6: Reduced M82 Images

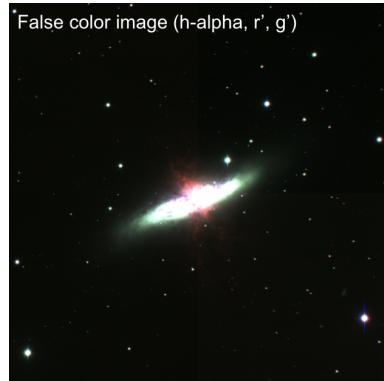


Figure 7: False-color Image of M82 using g' , r' , h-alpha filters

Each pixel in the FITS images contains a certain number of counts, which is related to the flux of photons received by the detector in the pixel. To calculate a calibration factor between the counts in the FITS file and a physical flux unit, we plotted known stars from the GAIA DR2 catalog, in green, and other stars in M101 of known magnitude under the various filters, in blue (figure 8).

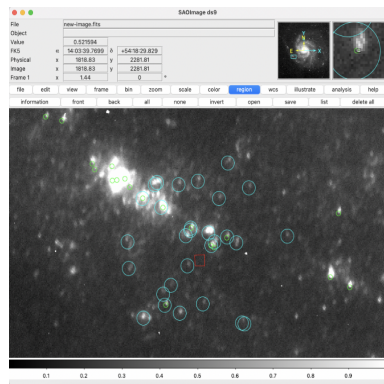


Figure 8: Candidate Stars of Known Magnitude for Flux Calibration (in green and blue circles)

2.2.3 Stellar Aperture and Background Annulus

We created an aperture around the star and an annulus roughly double the radius of the aperture away from the star to find the sum of counts from the star and to correct the stellar counts for the background noise using the counts in the annulus. To pick an optimal aperture radius, we computed the counts per second (image divided by the exposure time) across a range of aperture radii from 0 to 50. We defined the annulus to have inner radius twice the aperture radius and a width equal to the aperture radius.

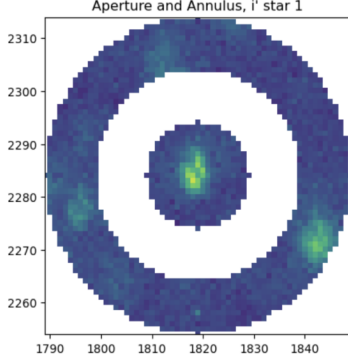


Figure 9: Aperture and Annulus Example for Star Calibration under the i' Filter



Figure 10: Plots for determining optimal aperture radius (in red)

We then used the zero-magnitude flux densities under the corresponding filter to convert the known magnitude of the star into a physical flux value using the following equation:

$$m = -2.5 \log_{10}\left(\frac{F}{F_0}\right) \quad (2)$$

where m is the magnitude of the star, F is the flux of the star in $W \cdot m^{-2} \cdot \mu m^{-1}$ and F_0 is the zero-magnitude flux density under the appropriate filter. Once we found the flux, we divided the flux by the brightness of the aperture (in counts/sec) to obtain our calibration factor. We calculated the calibration factors under each filter as follows:

i'	g'	r'	$h\text{-alpha}$
4.997e-22	3.446e-20	4.242e-22	6.176e-22

Table 1: Photometric calibration factors ($W \cdot m^{-2} \cdot \mu m^{-1}$ / (counts / sec))

3 Supernova 2023ixf

3.1 Background

A supernova is a bright explosion caused by the gravitational collapse of a star which has reached the end of its lifetime. At the core of massive stars, a large amount of heat and energy is being produced

via nuclear processes such as fusion. This causes the outward pressure near the core to be high, which counterbalances the force of gravity, which holds the star together, pushing inwards and therefore prevents the star from collapsing on itself. As material in the core runs out near the end of the star's life, the star begins to cool which reduces the internal pressure and when the pressure is low enough, gravitational collapse occurs. The Chandrasekhar limit, which is typically taken to be around 1.4 solar masses, defines the mass above which a collapsing star will produce a supernova as opposed to a white dwarf (1).

Supernovae can be classified as type I or type II. Type II supernovae are formed by the process described above when a massive star undergoes a rapid core collapse and subsequent explosion, sometimes even leaving a black hole behind if the mass is above 2 to 3 solar masses (3). Type I supernovae can further be classified as Type 1a, 1b and 1c. Type 1a supernovae occur mainly in binary systems containing at least one Earth-sized white dwarf. The more massive star grows and becomes too large to hold all the gas, so some of the material accretes onto the second star in the system. Eventually, the white dwarf mass becomes so large it undergoes core collapse, which also causes the other star to be ejected further away.

3.2 Goals

The supernova 2023ixf in M101 was classified as a type II supernova, meaning that the progenitor star was a super-massive star that underwent a rapid core collapse under its own gravitational force. Given that we imaged the galaxy under a wide range of filter wavelengths less than two weeks prior to the supernova's discovery, we analyzed our images to try and identify a progenitor star in the supernova region.

3.3 Image Analysis

To analyze the supernova region, we first found an astrometric calibration for the image to convert pixels to right ascension and declination values, then opened the calibrated FITS file in the DS9 software and plotted a box with side length 3 arcseconds centered at the coordinates of the supernova, which was 14:03:38.580 (RA), +54:18:42.10 (Declination) as shown in Figure 9.

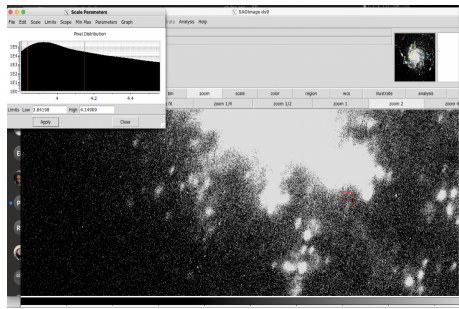


Figure 11: Region (in red) plotted on the i' M101 image

Since there was a lot of noise in the supernova region and it was difficult to visually make out a clear point source for the progenitor star, we adjusted our goal to instead calculate an upper bound for the magnitude of the progenitor star. A possible candidate for the progenitor was identified in an archival F814W image from the Hubble Space Telescope with magnitude 24.41 ± 0.06 (6). Since the i' filter covers the closest range of wavelengths to F814W out of all the filters we used, we focused on the i' exposures.

To compute the upper bound of the supernova region's magnitude, we used a similar process as specified in the Photometric Calibration section. We found the brightest pixel center of the region and defined an annulus and aperture around this center to find the total number of counts in the aperture and adjust it for the background counts in the annulus, and then we multiplied it by the calibration factor for the i' filter (listed in Table 1). We obtained a magnitude of 23.77, which is consistent with

the reported magnitude of 24.41, as a magnitude of 23.77 in the region indicates that we would not be able to see anything fainter than that, including the progenitor candidate since a 24.41 magnitude star is fainter than a 23.77 magnitude star.

4 Star Formation

4.1 Background

4.1.1 Star Formation Rate Indicators

The h-alpha emission line is produced when young massive stars ionize hydrogen gas (7). Because it is one of the strongest emission lines indicative of star formation, we often look for h-alpha emissions as a tracer for star-forming regions.

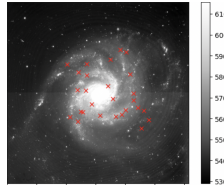
4.1.2 Goals

Our goals were to analyze the h-alpha regions to estimate the fraction of the galaxy undergoing massive star formation. Since the wavelengths covered by the h-alpha filter overlap with r' , we subtracted the reduced r' filter image from the reduced and scaled h-alpha image to isolate the portions that were unique to h-alpha. We also calculated the flux of a couple stars throughout the galaxy under the r' and i' filters to construct a color-magnitude diagram using the difference between the magnitudes of the star under both filters.

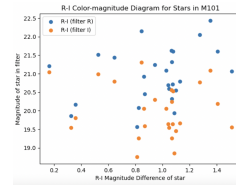
4.2 Observations

4.2.1 Color-Magnitude Diagram

We loaded the FITS files and picked random stars all throughout the galaxy and calculated the flux values using the calibration factors for each filter listed in Table 1.



(a) Chosen Stars for Flux Calculations



(b) R-I Color-magnitude Diagram

There isn't a very clear trend to the stars, but it seems that the magnitudes are higher overall under the r' filter versus the i' . Most stars are between magnitude 19 and 22.

4.2.2 Star Formation

To obtain an isolated-h-alpha image of M101, we scaled both h-alpha and r' exposures by subtracting the minimum pixel value from all pixels and dividing the image array by the maximum pixel value. This resulted in pixel values ranging from 0 to 1. We then subtracted the r' exposure from h-alpha (figure 13).

We see a very dark hole in the center, which is typically where older stars of the galaxy lie, while the arms of the spiral contain the most h-alpha (whiter areas correspond to higher counts), which is consistent with the fact that most star formation takes place in the arms of spiral galaxies.

We then set a threshold of around 0.27 counts (1 is the whitest and the maximum pixel value) to filter which pixels contained sufficient counts to be considered a pixel containing evidence of h-alpha emission in both the subtracted image as well as the reduced r' image and divided the total number of h-alpha pixels from the subtracted image by the number of h-alpha pixels in r' . We found that around

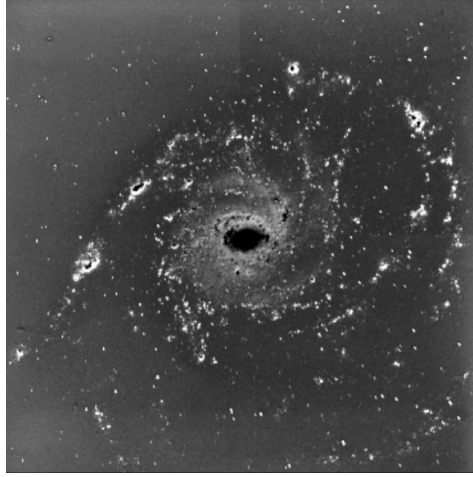


Figure 13: M101 isolated h-alpha regions

11% of the galaxy is currently undergoing massive star formation. This process is illustrated in more detail in section 5.1 for M82.

5 M82: The Cigar Galaxy

M82 is a starburst galaxy, meaning it contains a extremely high rate of star formation. Because of its proximity to neighboring galaxy M81, it experiences gravitational interactions with the galaxy which cause the exceptionally high rate of star formation. We will compare the fraction of the galaxy undergoing star formation in M82 with that of M101.

5.1 Star Formation

We used a similar technique as done for M101 images where we isolated the h-alpha emissions by subtracting the r' filter from the h-alpha image. The result is shown in figure 14.

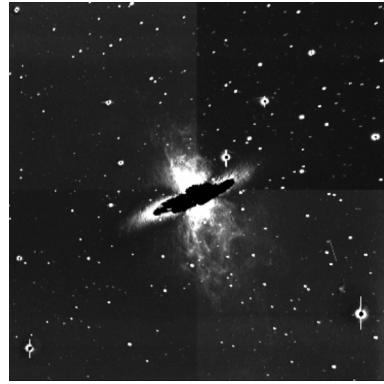
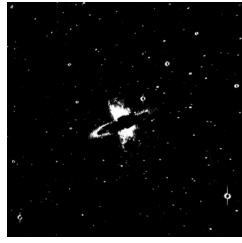
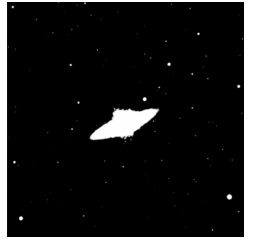


Figure 14: H-alpha Isolated Image of M82

Evidently, the central area of the disk has little to no star formation occurring. We see that the central bulge is very bright under the h-alpha filter, along with the edges of the disk, which indicate that those are the main star-forming regions. Based on a rough threshold of counts in a pixel that are considered to contain h-alpha emission, we set all pixels that pass this threshold to value one and all other pixels without any signal to have value 0. A visualization is presented in figure 15.

The ratio of the signals between the images is around 0.57, indicating that roughly 57% of the galaxy



(a) Pixels with signal from h-alpha filter (in white) (b) Pixels with signal from subtracted image (in white)

Figure 15: Signal extracted from images

is undergoing massive star formation. This value is significantly higher than the 11% calculated for M101, which makes sense as M82 is a starburst galaxy while M101 is not.

6 Sources of Error

Our method of estimating the fraction of the galaxy undergoing star formation comes with potential sources of error. We estimated a threshold to filter out pixels without enough noise to be considered a contribution to h-alpha emission, but this threshold was not exact and changing it by even 0.1 (pixel values were between 0 and 1) caused the percentage to be changed by 10%. Furthermore, there are some stars in the background with h-alpha emission which are also counted as part of the total amount of signal that was used when calculating the fraction. This is especially significant in M82, since M82 did not fill the entire field of view of the telescope, so background stars were factored into the calculation, while M101 was larger than the field of view so the majority of the stars in the image belonged to M101 itself.

7 Conclusions

Our analysis was consistent with reported candidates for the progenitor of the supernova. We calculated an upper bound of 23.77 for the magnitude of the star, while the reported value was a fainter magnitude of 24.41. We also found that roughly 11% of M101 was undergoing massive star formation, as compared to the 57% of M82. This is also consistent with the fact that M82 is a starburst galaxy. We observe that M101's star formation rate is much lower than M82, which suggests that it does not have as much gravitational interaction with nearby galaxies. M101 is part of a galaxy cluster, so gravitational interaction likely plays a role in the amount of star formation which is especially concentrated near the edges of the galaxy closer to neighboring galaxies, but is not as influential as it is in a starburst galaxy like M82.

References

1. [The Chandrasekhar Limit: Why Only Some Stars Become Supernovas](#)
2. [What is a supernova?](#)
3. [Gravitational Wave Physics](#)
4. [The Pinwheel Galaxy](#)
5. [Star Cluster Formation and Evolution in M101](#)
6. [Candidate Progenitor for Supernova 2023ixf](#)
7. [Star Formation Reference Survey](#)